

Advances in n-Type Chemical Vapor Deposition Diamond Growth:
Morphology and Dopant Control

Peer-reviewed author version

ROUZBAHANI BAYATANI, Rozita; KAMATCHI JOTHIRAMALINGAM, Sankaran;
POBEDINSKAS, Paulius & HAENEN, Ken (2024) Advances in n-Type Chemical
Vapor Deposition Diamond Growth: Morphology and Dopant Control. In: Accounts of
Materials Research,.

DOI: 10.1021/accountsmr.3c00273

Handle: <http://hdl.handle.net/1942/42795>

Advances in *n*-type chemical vapor deposition diamond growth:

Morphology and dopant control

Rozita Rouzbahani^{*1}, Kamatchi Jothiramalingam Sankaran²,

Paulius Pobedinskas¹, and Ken Haenen^{*1}

¹*Institute for Materials Research (IMO), Hasselt University, and IMOMEC, IMEC vzw,*

Wetenschapspark 1, 3590 Diepenbeek, Belgium

²*CSIR-Institute of Minerals and Materials Technology, Bhubaneswar-751013, India*

E-mails: rozita.rouzbahani@uhasselt.be, and ken.haenen@uhasselt.be

Conspectus

Diamond, a wide bandgap semiconductor, has captivated researchers for decades due to its exceptional properties. While *p*-type doping has dominated the field, the advent of *n*-type diamond, doped by nitrogen or phosphorus, has unlocked novel prospects for diverse applications. Nonetheless, the chemical vapour deposition (CVD) of *n*-type diamond faces substantial hurdles, particularly concerning crystalline quality and dopant concentration control. In this Account, we summarize our progress in developing high quality CVD *n*-type diamond films. Our research initiates with nitrogen introduction into the CH₄/H₂ CVD plasma for depositing polycrystalline diamond films. The addition of 4% N₂ gas induces the formation of ultra-nanosized diamond grains through CN species, but further increases in nitrogen content result in grain agglomeration into larger sizes. Fixing 3% of N₂ in the CVD plasma, we explore the influence of methane concentration on N-doped nanocrystalline diamond (NCD) films. At a low methane concentration of 1%, faceted diamond grains are formed, while increasing methane to 15% yields nanoneedles encased in nanographitic phases, featuring a low resistivity of 90 Ω·cm. We further investigate P-doped polycrystalline diamond films, where preliminary examinations of P-doped NCD reveal well-defined grain structures but also morphological imperfections and twin boundaries, with a phosphorus incorporation of $\approx 10^{19}$ cm⁻³. Our investigations also cover P-doped (110)-textured polycrystalline CVD diamond films, finding that the phosphorus concentration varies with grain misorientation and that higher phosphine concentrations lead to a more uniform distribution. Additionally, we note that an increase in

the [P]/[C] ratio in the CVD plasma of P-doped diamond growths leads to the transformation of NCD to ultra-NCD, reducing residual stress, and affecting film quality. In a complementary investigation, we explore the co-doping of NCD films with nitrogen and phosphorus, observing a transition from micron-sized faceted diamond grains to nano-sized grains with increasing nitrogen content at a fixed amount of phosphorus concentration in the CVD plasma.

Exploring diamond's potential as a semiconductor, our research group investigate the captivating properties of P-doped single crystal diamond films, given a shallower donor energy level of 0.6 eV compared to nitrogen's deep donor level at 1.7 eV. Our findings indicate optically active defects with various electronic levels, using a doping range from 10^{16} to 10^{19} cm^{-3} in (111)-oriented P-doped diamond epilayers. However, challenges like formation of defects, persist for this orientation. In contrast, (100)-oriented diamond films are renowned for the *p*-type conductivity and high crystalline quality, though achieving *n*-type conductivity remains a challenge. Our research highlights the critical role of varying methane concentration during CVD in influencing both crystalline quality and phosphorus concentration. Elevated methane concentrations are found to induce surface degradation, affecting film quality and doping level. Surprisingly, (110)-oriented P-doped single crystal diamond growth demonstrates promising results with a 33 $\mu\text{m/h}$ deposition rate using only 1% methane concentration. Furthermore, the off-angle from the (110) orientation can potentially impact film quality, indicating by cathodoluminescence spectroscopy, offering exciting prospects for future research.

The insights provided in this Account will illuminate the CVD growth of *n*-type diamond films, contributing to the advancement of diamond-based devices.

1. Introduction

Diamond, an extraordinary material with unparalleled properties, holds great potential for a wide array of applications, including power electronics, quantum technologies, and biotechnology¹⁻³. Its electrical and thermal properties surpass those of alternative wide bandgap semiconductors such as 4H-SiC or GaN⁴. With its exceptional electron and hole mobility, along with remarkable resistance to irradiation, diamond is an ideal choice for detectors⁵. In addition to these properties, diamond possesses a unique capability to host various impurities bringing forth interesting electrical and optical characteristics.

The completely sp^3 -hybridized diamond with a wide bandgap of 5.47 eV is a distinctive insulator with its resistivity reaching roughly $10^{12} \Omega \cdot \text{cm}$. In this form, diamond cannot be effectively utilized for most electronic applications unless it undergoes a successful conversion into a semiconductor. In order to enhance the conductivity of diamond films, a common approach involves doping them with group V atoms such as nitrogen or phosphorus, elements with five electrons in their valence shell result in n -type doping^{6,7}. Conversely, the introduction of group III atoms, e.g. boron with three valence electrons, into the diamond lattice leads to p -type doping. In case of p -type diamond, the covalent radius of boron (0.88 Å) closely matches that of carbon (0.77 Å), while its energy level has been measured at approximately 0.37 eV above the valence band maximum. As a result, achieving p -type doping in diamond is considered easily attainable. On the other hand, with a negative formation energy (-3.4 eV), nitrogen readily enters the diamond lattice to create n -type doping. However, its interaction with the surrounding carbon atoms leads to one of the N-C bond lengths elongating compared to the original C-C bond length and is longer than the other three N-C bonding⁸. This results in a significantly deep donor level (1.7 eV), rendering it impractical for semiconductor devices operating at room temperature. As the second option, phosphorus is characterized by a considerably larger covalent radius (1.06 Å), and a high positive formation energy (6.67 eV). Recent pioneering works have shed light on phosphorus incorporation into diamond, revealing a relatively deep donor level (0.6 eV), albeit shallower in comparison to nitrogen^{9,10}. In addition, co-doping strategies have been suggested with the aim of improving the properties of the diamond films. For instance, Miyazaki *et al.* reported, based on *ab initio* calculations, that the N-H-N complex in diamond shows a much shallower donor character compared to an isolated nitrogen donor¹¹. Later, Lombardi *et al.* conducted a comprehensive investigation into the interaction of H with B, P, and Si in diamond, revealing it is energetically favourable for hydrogen to be trapped and to passivate boron and phosphorus¹².

Recently, significant advancements have been reported in the growth of high quality doped diamond through various techniques including chemical vapour deposition (CVD) and high-pressure high-temperature (HPHT) synthesis. Meanwhile, the production of man-made single- and polycrystalline diamonds have developed to high levels. The quality of diamond films grown by the CVD method spans from ultra-pure and defect-free to conductive, doped with boron, phosphorus, etc., and quantum-grade diamond leveraging single defects such as the renowned nitrogen-vacancy (NV) colour centre. Prototype devices have been successfully implemented across different fields of applications^{13,14}.

In this Account, our primary focus centres on the CVD growth of *n*-type diamond by nitrogen and phosphorus, spanning from polycrystalline to single crystal diamond, a core endeavour of our research group since its inception. We place particular emphasis on investigating morphology, crystalline quality, and the doping process. To conclude, we discuss challenges and opportunities inherent to this field.

2. *N*-type diamond

N-type diamond has garnered significant attention in recent years. By carefully introducing impurities during the growth process, such as nitrogen or phosphorus, the diamond lattice can be modified to possess an excess of electrons, enabling it to function as an efficient semiconductor. In this Account, we investigate the research findings from our group on the CVD growth parameters and unique properties of N-, P-, and co-doped diamond films in different forms. To facilitate this examination, we employed an array of characterization techniques, including optical spectroscopies and electron microscopies. Here, we proceed to present and discuss these significant findings, with a particular focus on elucidating the electrical and optical properties of the *n*-type diamond, while highlighting its potential as a promising semiconductor material.

2.1 Polycrystalline *n*-type diamond

2.1.1 Nitrogen-doped diamond films

2.1.1.1 Introduction of N_2 in CH_4/H_2 CVD plasma

Tailoring the growth parameters of diamond film deposition can alter the morphology, microstructure and bonding characteristics of the films. Particularly, the existence of

sp^2 -bonded carbon such as graphite and amorphous carbon within sp^3 -bonded carbon (the diamond) matrix are the important factors in determining several characteristics of the material. Sankaran *et al.* demonstrated that systematic change in the ratio of N_2 in the CH_4/H_2 plasma controls the surface morphology, microstructure and bonding structure of polycrystalline diamond films¹⁵. By increasing the concentration of N_2 from 0% to 4%, the diamond grain size changes from faceted grains of size 100 nm for 0% N_2 (Fig. 1(a)) to a roundish granular structure for 1% N_2 (Fig. 1(b)) and to 10 nm ultrananocrystalline diamond (UNCD) grains for 4% N_2 (Fig. 1(c)). Further increasing the concentration of N_2 to 8%, an increase in the size of the diamond grains is observed, but also a certain degree of porosity is introduced in the films (Fig. 1(d)). The incorporation of N_2 in the plasma also rapidly decreases the growth rate of the diamond films, which is due to the presence of CN radicals in the plasma, reducing the concentration of CH_3 radicals, consequently causing a decrease in the growth rate^{16,17}. In addition, the electrical resistivity of the diamond films, measured using the 4-point probe technique, reveals that the resistivity of the diamond films without nitrogen is nearly $> 7.1 \times 10^4 \Omega.cm$. As the concentration of N_2 increases, the resistivity exhibits a decreasing trend. Once N_2 concentration stands at 4%, the resistivity drops to 74 $\Omega.cm$, whereas at higher nitrogen concentrations, the film resistivity rises again to about $4.3 \times 10^3 \Omega.cm$ for the diamond film with 10% N_2 concentration.

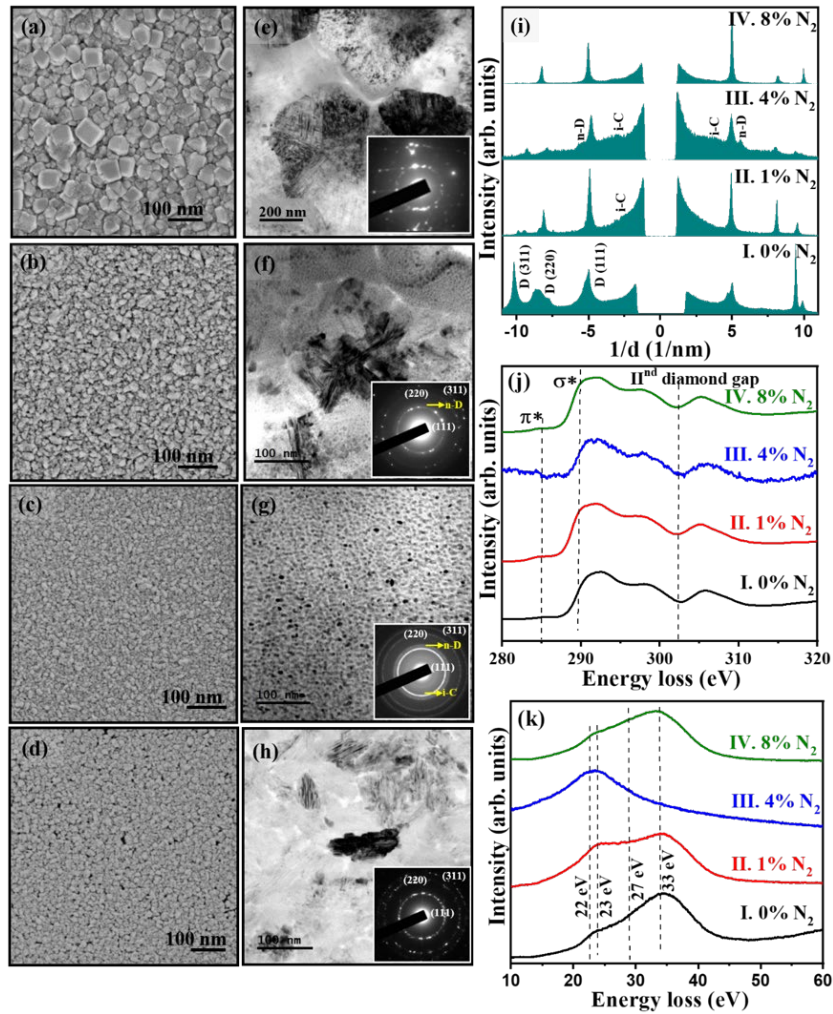


Figure 1: (a-d) Scanning electron microscopy (SEM) and (e-h) transmission electron microscopy (TEM) micrographs of diamond films grown using (a, e) 0%, (b, f) 1%, (c, g) 4%, and (d, h) 8% N_2 concentrations. Typical (i) liner diffraction pattern, (j) core-loss, and (k) plasmon-loss electron energy loss spectroscopy (EELS) spectra of I. 0%, II. 1%, III. 4%, and IV. 8% N_2 . Reproduced with permission from ref 15. Copyright 2015 American Institute of Physics.

The TEM image of 0% N_2 films, shown in Figure 1(e), displays high contrast grains oriented near the zone-axis. Incorporation of N_2 in CH_4/H_2 plasma noticeably modifies the microstructure of the diamond films. Predominantly, the microstructure of 4% N_2 films (Fig. 1(g)) illustrates that the clusters in the films consist of randomly oriented 5 nm sized spherical diamond grains with clear grain boundaries. A thorough investigation of the selective area electron diffraction (SAED) pattern (inset, Fig. 1(g)) discloses clear diffraction rings related to (111), (220), and (311) lattice planes of diamond. Moreover, a faint diffraction ring of smaller size than the $(111)_D$ ring corresponds to i-carbon (i-C) phase, the bcc structured carbon with cell parameter $a_0 = 0.432$ nm as well as a diffraction ring with the size slightly larger than the $(111)_D$ ring represents n-diamond (n-D) phase, the fcc structured carbon with $a_0 = 0.356$ nm^{18,19}. Furthermore, a prominent diffused ring at the centre of SAED indicates the presence

of sp^2 phases in these films. In contrast, when the N_2 is further raised to 8%, the grains are agglomerated and form a few hundred nanometer sized large elongated aggregates (Fig. 1(h)). The linear diffraction patterns (Fig. 1(i)) derived from the SAED patterns (insets, Figs. 1(e-h)) finely demonstrate the origin of nano-sized particulates such as n-D and i-C phases among the diamond particulates when N_2 is incorporated in the CH_4/H_2 plasma. Once N_2 concentration increases (4% N_2), the proportion of nano-sized particulates increases (spectrum III, Fig. 1(i)). Further increase in N_2 content (8%) converts the n-D and i-C particulates into diamond structure (spectrum IV, Fig. 1(i)).

The significant changes in the bonding structure of diamond films due to the N_2 -addition are further examined using TEM-EELS. The carbon edge core-loss EELS spectra (Fig. 1(j)) corresponding to these diamond films indicate that, for all of the diamond films, there is a notable sharp increase near 289.5 eV (σ^* -band) and a significant dip in the vicinity of 302 eV, implying the diamond nature of the samples^{20,21}. Moreover, there is a σ^* -band at 284.5 eV in core-loss EELS spectra of spectrum II to IV, indicating the induction of sp^2 -bonded carbon due to the addition of N_2 in the plasma. Notably, the σ^* -band for the 4% N_2 films (spectrum III, Fig. 1(j)) is not as sharp when compared to the spectra for other films, indicating that there is larger proportion of defects contained in the diamond lattices. The plasmon-loss EELS spectra, shown in Figure 1(k), clearly differentiate the crystalline and non-crystalline forms of carbon in the N_2 -incorporated diamond films. Typically, the peak appears at 27 eV indicate the graphitic phase, whereas the peaks appear at 23 and 33 eV designate the diamond phase²⁰. In case of 4% N_2 films, a broad peak observed at 22 eV attributes to the formation of n-D and i-C in the films (spectrum III, Fig. 1(k))²⁰. The optical emission microscopy confirms that the plasma of $CH_4/H_2/4\%N_2$ exhibits the highest concentration of CN and C_2 species. Therefore, the CN and C_2 species in the plasma are the main decisive factors for the microstructural evolution with the N_2 concentration, ensuing in the formation of ultra-nanosized diamond grains with broad grain boundaries enclosing sp^2 phases, together with the n-D and i-C particulates. The sp^2 phases in the grain boundaries of 4% N_2 films lead to easy conduction of electrons, resulting in the lowest resistivity of these films.

2. 1.1.2 *One-dimensional needle-like N-doped nanocrystalline diamond films*

Methane not only provides a carbon source for the growth of diamond, it also has an essential role in the evolution of microstructure in the nitrogen-incorporated NCD films synthesized using a $CH_4/H_2/N_2$ plasma^{22,23}. Several reports have highlighted that an increase in the

concentration of CH₄ leads to a conversion from micron-sized diamond grains to nano-sized diamond grains^{24,25}. Badzian *et al.* reported that the diamond growth was not facilitated at low CH₄ concentration and once the methane concentration increased, the growth of diamond grains was observed²⁶. Our research group reported the morphological variation in the N-incorporated NCD films with increase in the CH₄ concentration using a CH₄/H₂/3%N₂ microwave plasma²⁷. With 1% CH₄ concentration, the films contain ~ 600 nm sized randomly oriented rough faceted diamond grains (Fig. 2(a)). Upon increasing the concentration of CH₄ to 5% and 10%, the morphology changes to cauliflower-like structured grains of size about 200 nm to 20 nm (Figs 2(b) and (c)). However, at 15% CH₄ concentration, one-dimensional randomly oriented needle-like structured grains are achieved. The length of these needles is about 50–250 nm with a diameter of a few nanometers (Fig. 2(d)). The growth rate and substrate temperature increase with increase in CH₄ concentration. Particularly, the growth rate and substrate temperature for the needle-like morphological NCD films grown at 15% CH₄ are (33.5 ± 0.9) nm/min and $\approx 780^\circ\text{C}$, respectively. Moreover, with increase in CH₄ concentration, a decrease in the resistivity values is observed and attaining a low resistivity value of $90 \Omega \cdot \text{cm}$ for the films grown using 15% CH₄ concentration. The bonding characteristics of these NCD films investigated by Raman spectroscopy reveal that with increase of CH₄ concentration, the diamond peak diminishes and the sp²-bonded carbon in these materials increases (Fig. 2(e)). The two-dimensional band around 2709 cm^{-1} signifies evidently the existence sp²-bonded nanographitic phases in 15% CH₄ NCD films.

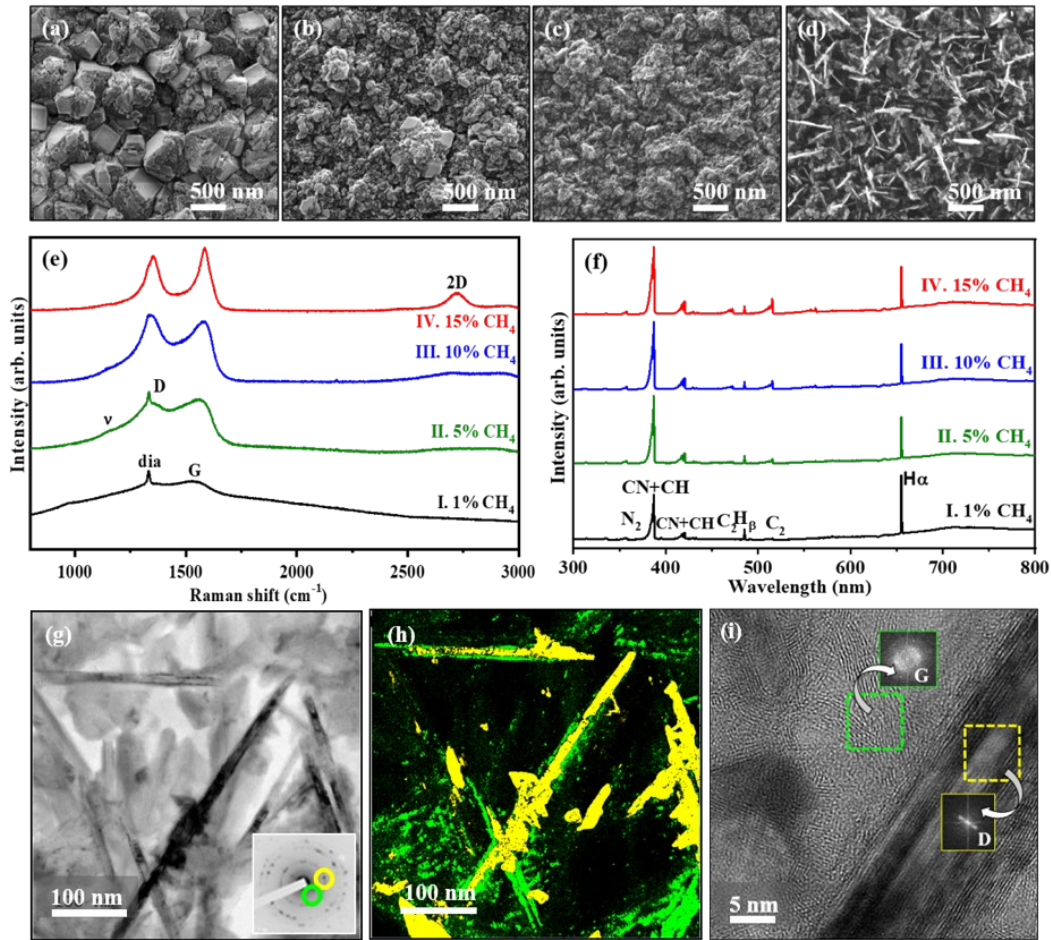


Figure 2: SEM micrographs of NCD films grown using (a) 1%, (b) 5%, (c) 10%, and (d) 15% CH₄ concentrations in CH₄/H₂/3%N₂ plasmas. (e) Raman spectroscopy and (f) optical emission spectroscopy spectra of I. 1%, II. 5%, III. 10%, and IV. 15% CH₄. (g) Bright-field (BF), (h) dark field (DF) TEM micrographs, and (i) structure image of NCD films grown using 15% CH₄ in CH₄/H₂/3%N₂ plasmas, describing the evolution of needle-like diamond-graphite core-shell granular structure. Reproduced from ref 27. Copyright 2016 American Chemical Society.

From TEM investigations, it is observed that the films grown at 15% CH₄ concentration (Fig. 2(g)) shows the evolution of anisotropic growth of needle-like granular structured diamond grains with branching characteristics. Figure 2(h) provides a clear DF TEM micrograph of the films, distinctly illustrating the evolution of needle-like diamond grains (yellow) with graphitic phases (green) encompassing them. A core-shell microstructure is observed in the structure image of 15% CH₄ NCD films (Fig. 2(i)). The needle-like diamond grains are encased by a few atomic to 10 layered thick graphitic phases. Many groups have observed such kind of microstructure on diamond films^{23,28}. Additionally, the Fourier transformed images in the inset of Figure 2(i) prove the existence of diamond and graphite, respectively. These results clearly elucidated the role of CH₄ in the evolution of morphology, microstructure, and bonding characteristics of CH₄/H₂/3%N₂ grown NCD films, especially the origin of diamond-graphite core-shell needle-like structure that lead to the improved electrical

conductivity of 15% CH₄ NCD films. The CN species present in the plasma have a significant role in the formation of needle-like granular structure for the 15% CH₄ NCD films (Fig. 2(f)). The substrate temperature is 780°C for 15% CH₄-containing plasmas, which is favourable to the CN species to preferentially attach to the C₂ species and induce anisotropic diamond growth, resulting in the formation of needle-like diamond grains with high aspect ratio. In addition, during this growth, the C atoms at the surface of sp³-bonded diamond tend to form sp²-bonded graphitic phases, hence forming a diamond-graphite core-shell structure. The presence of graphitic phases facilitates the electron transport ensuing enhanced electrical properties of 15% CH₄ NCD films.

2.1.2 Phosphorus-doped diamond films

The P-doped polycrystalline diamond films have been investigated extensively²⁹⁻³². In the examination of NCD P-doped samples, deposited with a 10000 ppm [P]/[C] ratio in the gas phase of CH₄/H₂/PH₃, we observed homogenous films with well-defined grains (Fig. 3(a)), and a notably low sp²/sp³ ratio, as validated by Raman spectroscopy. Nevertheless, the annular DF (ADF)-TEM imaging (Figs 3(b-c)) unveiled certain morphological imperfections, such as notched edges and facets, and $\Sigma = 3\{111\}$ twin boundaries. Analysing the secondary-ion mass spectroscopy (SIMS) results of a 1.1 μm thick film (Fig. 3(d)) determined a phosphorus concentration on the order of 10¹⁹ cm⁻³, with a significant fraction integrated at substitutional donor sites. Using carbon and phosphorus maps obtained by energy-dispersive X-ray TEM, we observed that the phosphorus signal closely follows the carbon signal, indicating an incorporation of phosphorus into the diamond lattice with a small enrichment of phosphorus at grain boundaries, certainly not systematic.

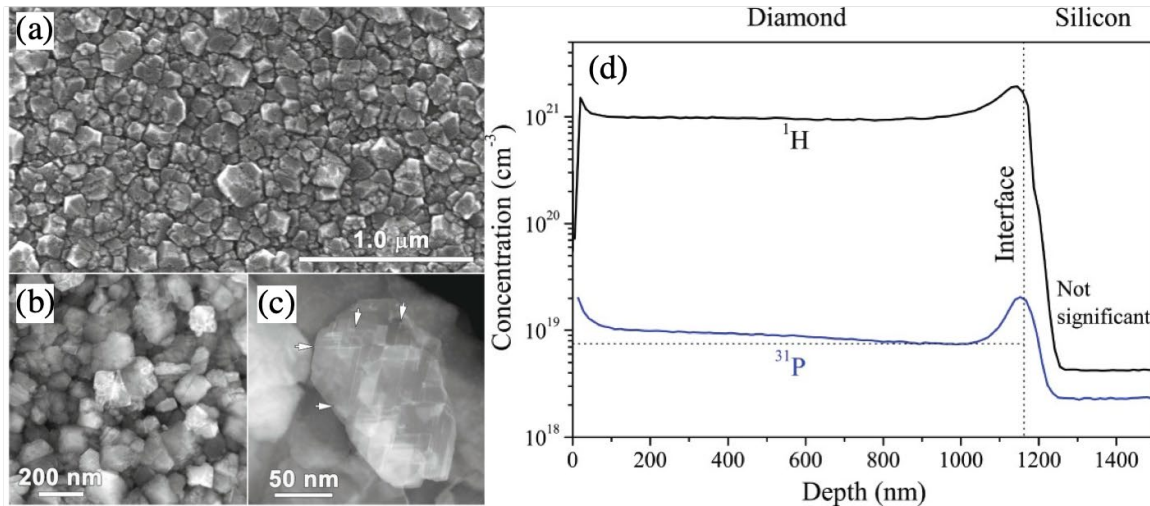


Figure 3: (a) SEM image of a 320 nm thick P-doped NCD film grown at 10000 ppm [P]/[C] ratio in the plasma feed gas. (b) Low magnification ADF-TEM image, showing randomly oriented diamond grains. (c) ADF-TEM image of a selected diamond grain. Arrows indicate $\Sigma = 3\{111\}$ twin boundaries. (d) SIMS data of the 1.1 μm thick P-doped NCD layer on Si. The dotted horizontal line marks $7.5 \times 10^{18} \text{ cm}^{-3}$. Reproduced with permission from ref 30. Copyright 2014 WILEY-VCH verlag GmbH & Co. KGaA, Weinheim.

Furthermore, we studied the formation of P-doped (110)-textured microcrystalline CVD diamond films³². When employing low phosphorus concentrations (≤ 200 ppm), the local dopant incorporation can vary over three orders of magnitude, depending on the grain misorientation with respect to the perfect [110] direction. A lower misorientation angle leads to a lower phosphorus concentration. Once this misorientation angle exceeds 10° , the formation of (111) microfacets occurs. Higher phosphine concentrations in the plasma seem to accelerate this process, leading to a more uniform distribution of phosphorus concentration. We also observed an increase in strain effects at higher phosphorus incorporation (500 ppm), together with a structural degradation³³.

Due to the limited scalability in conventional resonant cavity systems, in which single crystal CVD diamond layers are typically grown, the linear antenna microwave plasma-enhanced (MW PE CVD) system³⁴, which operates based on the surface wave plasma technique, is a promising alternative. Recently, we performed P-doping of NCD using a $\text{H}_2/\text{CH}_4/\text{CO}_2/\text{PH}_3$ plasma in this system³¹. We studied the morphological changes and associated residual in-plane stress of NCD thin films grown at various phosphine concentrations in the CVD plasma and substrate temperatures. It is seen that the film transforms from NCD to UNCD with increasing [P]/[C] ratio in the plasma, leading to decreased residual stress and with lower film quality (Fig. 4(a)). The consistent dendritic morphology continues for films fabricated in [P]/[C] = 8090 ppm conditions up to 800°C substrate temperature (Fig. 4(b)). With an increase

to 900°C, an unexpected change occurs in the film – the dendrite-like features become less distinct with vague grain boundaries and with even smaller grains.

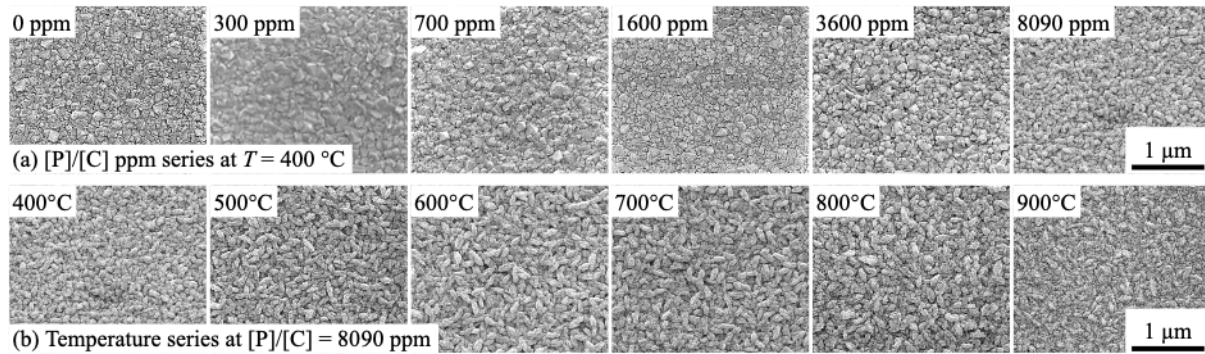


Figure 4: SEM images of the (U)NCD films: (a) [P]/[C] series at $T = 400^\circ\text{C}$ and (b) temperature series at [P]/[C] = 8090 ppm. All films were about 250 nm thick and were deposited under 5% CH_4 , 6% CO_2 , and 5 cm distance between the substrates and the linear antenna. Reproduced with permission from ref 31. Copyright 2024 Elsevier.

Similar to the surface morphology analysis by SEM, the Raman results showed little variation in diamond peak, D- and G-bands for the samples grown at a substrate temperature of 400°C with increasing [P]/[C] ratio from 0 ppm to 3600 ppm. At the highest [P]/[C] ratio of 8090 ppm, the Raman spectra corresponded to a typical UNCD spectra. The increase in substrate temperature (at [P]/[C] = 8090 ppm), showed as well little variation in the sp^2/sp^3 ratio, and only above 700°C, the increase in the sp^2/sp^3 ratio was observed. SIMS depth profiling was carried out on the sample deposited at [P]/[C] = 8090 ppm at a substrate temperature of 900°C. Results show phosphorus incorporation of $4.2 \times 10^{19} \text{ cm}^{-3}$ maintains uniform throughout the thickness of the diamond layer.

2. 1.3 Nitrogen and phosphorus co-doped diamond films

In the preceding sections, we have outlined the findings on the effects of nitrogen and methane in CH_4/H_2 plasma on the evolution of microstructure, particularly the formation of nanographitic phases in the grain boundaries that enhances the electrical properties of polycrystalline diamond films. However, it is worth noting that despite these improvements, the insulating nature of the diamond grains still restricts the electrical conduction to the grain boundaries. Conversely, the substitutional doping of phosphorus in diamond films makes the diamond grains electrically conductive. Consequently, we investigated the nitrogen and phosphorus co-doped NCD films deposited using MW PE CVD process. Our objective is to achieve electrical conductivity within the diamond grains through phosphorus doping, while simultaneously ensuring an improvement in the electrical conductivity by incorporating

nitrogen, due to the formation of nanographitic phases in the grain boundaries³⁵. The growth was carried out by varying the concentration of N₂ from 0.2% to 2% by keeping the CH₄ and phosphine (PH₃) concentrations constant. SEM observations indicate the presence of micrometer-sized faceted diamond grains in the case of 0.2% N₂ NCD films (Fig. 5(a)), whereas grains are drastically reduced to nano-metric scale when the nitrogen content is increased (Figs 5(b-d)). The 2% N₂ NCD films exhibit small cauliflower-like morphological diamond grains with abundant grain boundary phases (Fig. 5(e)). The sp²/sp³ ratio, assessed from the Raman spectra (Figs 5(f-g)), as a function of the nitrogen concentration indicates that the sp² phases increases with increasing nitrogen content, which tend to level off at 1%. Therefore, we conclude that the CN, C₂ and CH species have substantial impact on the formation of nano-sized diamond grains with abundant sp²-bonded carbon grain boundaries of the nitrogen and phosphorus co-doped NCD films.

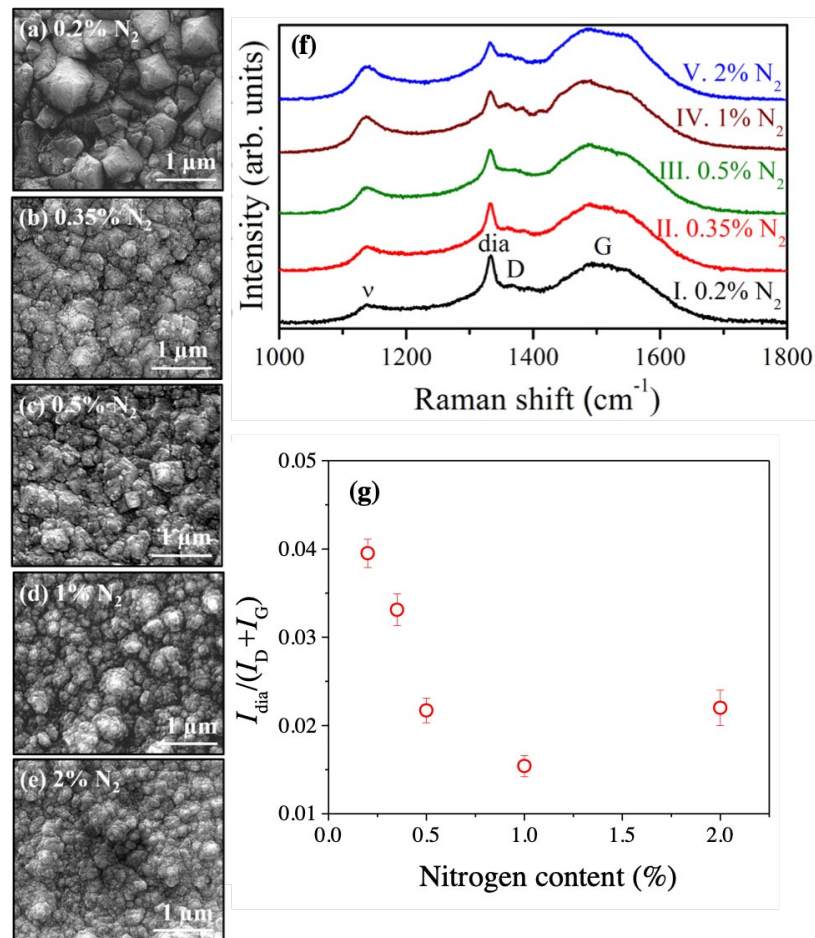


Figure 5: SEM micrographs of the nitrogen and phosphorus co-doped NCD films grown with (a) 0.2%, (b) 0.35%, (c) 0.5%, (d) 1%, and (e) 2% N₂. (f) Raman spectra of nitrogen and phosphorus co-doped NCD films growth using various N₂ concentrations. (g) The ratio of diamond (I_{dia}) and D- and G-band ($I_{\text{D}} + I_{\text{G}}$) peaks for each nitrogen content. Reproduced with permission from ref 35.

2.2 Single crystal *n*-type diamond

2.2.1 *P*-doped diamond films grown on different crystal orientations

2.2.1.1 (111) orientation

Phosphorus stands out as the most promising donor dopant due to its shallow donor energy level (0.6 eV). In 1997, Koizumi *et al.* successfully deposited single crystal *n*-type diamond thin films with varying dopant concentration, utilizing PH₃ as the dopant source³⁶. The resulting films exhibited an activation energy of 0.43 eV (a value that was adjusted to (0.60 ± 0.02) eV in later publications³⁷) and a Hall mobility of 23 cm²/V·s at approximately 500 K. Since then, numerous efforts have been devoted to the growth of high-quality single crystal *n*-type P-doped diamond films^{38,39}. In 1999, Koizumi *et al.* reported that the (111) orientation diamond emerged as the optimal substrate for the growth of P-doped diamond⁴⁰. The corresponding activation energy ranged around 0.55 eV, while the Hall mobility reached 28 cm²/Vs over a temperature range of 370 to 700 K. In the same year, Nesládek *et al.* presented spectroscopic evidence of the phosphorus optical activity for the first time in (111)-oriented P-doped diamond grown with a 1000 ppm of [P]/[C] ratio⁴¹. In that work, two optically active defects were revealed; one at 0.56 eV and the other one at around 0.81 eV. A comparative study was published by Haenen *et al.* on the same orientation of P-doped diamond films deposited at different [P]/[C] ratios of 1000 ppm and 500 ppm, with the donor concentrations of 5×10^{18} cm⁻³ and 3×10^{18} cm⁻³, respectively⁴². It was shown that the sample grown at 500 ppm exhibited less broadened oscillatory photocurrent spectra with more structured minima at temperature range between 4.2 to 77.4 K. In addition, they introduced four excited levels of phosphorus level (523, 563, 575, and 584 meV) above the phosphorus ground level by photothermal ionization spectroscopy. Subsequently, in alignment with the theoretical predictions made by Gheeraert *et al.*⁴³, our research group in 2004 reported a new electronic structure of phosphorus with more excited levels, using doping levels ranging from 10^{16} to 10^{19} cm⁻³ in (111)-oriented diamond films⁴⁴. Building upon these foundational works, *n*-type conduction in (111)-oriented P-doped diamond with high electron concentrations has been successfully obtained in recent years, making it a potential candidate for (opto)electronic applications⁴⁵. In addition, it has been reported that the electrical excitation of colour centres such as the silicon vacancy (SiV) is determined by electron and hole-capture processes, related to the density of free electrons and holes in the vicinity of the colour centre⁴⁶. Combining these two facts gives the possibility of fabricating a Schottky diode based on the creation of colour

centres in *n*-type diamond. However, there are challenges to overcome to obtain the conditions for single-photon emission in P-doped diamond, such as crystal structure distortion and degradation caused by the incorporation of the phosphorus atoms and photoluminescence related to P, N co-doping, which can suppress the signal-to-noise ratio and thus hinder single-photon emission. In a recent collaboration with Siegen University, the optical properties of SiV colour centres in (111)-oriented P-doped single crystal diamonds grown at different phosphorus concentrations were investigated to show the conditions for single-photon emission⁴⁷. It was shown that by removing nitrogen (< 1 ppb) from technical gases used for the CVD plasma of P-doped diamond, the luminescence background can be significantly suppressed even at high phosphorus concentrations ($[P]/[C] = 5000$ ppm) and the conditions for single-photon emission can be attained. However, the presence of crystal defects and dislocations is still a challenge for this orientation.

2.2.1.2 (100) orientation

As the (100)-oriented diamond substrates are known for their stability, high crystallinity, and favourable *p*-type conductivity, there has been significant attention focused on the CVD growth and characterization of P-doped layer on this orientation. The first *n*-type conductivity on (100)-oriented samples was reported by Kato *et al.* with an incorporation efficiency of about 0.02%, which is two-orders of magnitude lower than that of (111)-oriented P-doped layers⁴⁸. Preceding this breakthrough, the first photocurrent measurements were conducted on (100)-oriented P-doped diamond films with a low mobility of $10 \text{ cm}^2/\text{V}\cdot\text{s}$, where the presence of a defect level at approximately 0.85 eV was observed⁴⁹. The same defect level had previously been reported in (111)-oriented P-doped diamond layers⁵⁰. Since these pivotal observations, researchers have been mostly engaged in the quest to find a trade-off between the crystalline quality and the phosphorus concentration in P-doped single crystal diamond films. In CVD growth of diamond, it has been firmly established that methane concentration yields considerable influence over the resulting crystalline quality of the films. A low methane-to-hydrogen ratio ($\leq 0.5\%$) in the CVD plasma normally leads to a low density of defects in diamond layers. However, the low methane concentration (low growth rate) becomes impractical when the objective is to attain the necessary thickness for diamond films, typically in the range of a few tens of micrometers for power electronics. In addition, our research group has previously reported an increase in the doping concentration of *p*-type diamond associated with higher methane content⁵¹. On the other hand, elevating the methane concentration causes

the appearance of several types of spontaneous imperfections in the diamond lattice structure, such as dislocations. Therefore, we conducted a study on (100)-oriented P-doped diamond films which were deposited at various methane concentrations (1.5%, 2.5%, and 3.5%) in the CVD plasma feed gas⁵². We found a different growth mechanism for each of the used methane concentration. As can be seen in Figures 6(a-c), the average roughness of the samples, estimated by atomic force microscopy (AFM), increased from 15.8 to 129 nm by increasing the methane concentration from 1.5% to 3.5% in the plasma. Furthermore, the roughness values indicate a change in the growth mechanism; the sample grown at 1.5% methane concentration displayed stepped-flow lateral growth, whereas the samples grown at the higher methane concentrations exhibited three-dimensional growth. In order to estimate the phosphorus concentrations in the films, we characterized the layers by cathodoluminescence (CL) spectroscopy. It was demonstrated that the phosphorus content marginally decreases with increasing methane concentration, while the concentration of phosphorus containing gas (PH₃) remains constant (3333 ppm) in the plasma. We proposed that this observation in (100)-oriented P-doped diamond films could be related to the higher growth rates at higher methane concentrations, since phosphorus atoms tend to segregate towards the surface⁴⁸. Additionally, a 7 μm-thick P-doped diamond film, deposited with 1.5% methane concentration on a (100)-oriented heavily (*p*⁺) and lightly (*p*⁻) B-doped diamond stack layer (*p*⁺/*p*⁻), was studied by CL spectroscopy. The CL measurements were performed on an extracted lamella from the *n*-type layer at varying distances from its surface, corresponding to different depths in the P-doped layer. The doping concentration at different places was found to be $3.5 \times 10^{17} \text{ cm}^{-3}$, which is an order of magnitude greater than the value obtained from the sample grown at the same growth conditions, but on a HPHT substrate. Furthermore, a second lamella with a thickness of $\approx 15 \text{ μm}$ was fabricated to study the entire *p*⁺/*p*⁻/*n* stack layer by TEM. As observed in Figures 6(d-e), the layer is replete with $1/2a\langle 110 \rangle$ burger vector dislocation and stacking faults with $1/3\langle 111 \rangle$ displacement vector, unlike findings in the same P-doped layer grown on the HPHT substrate, where no defects were reported.

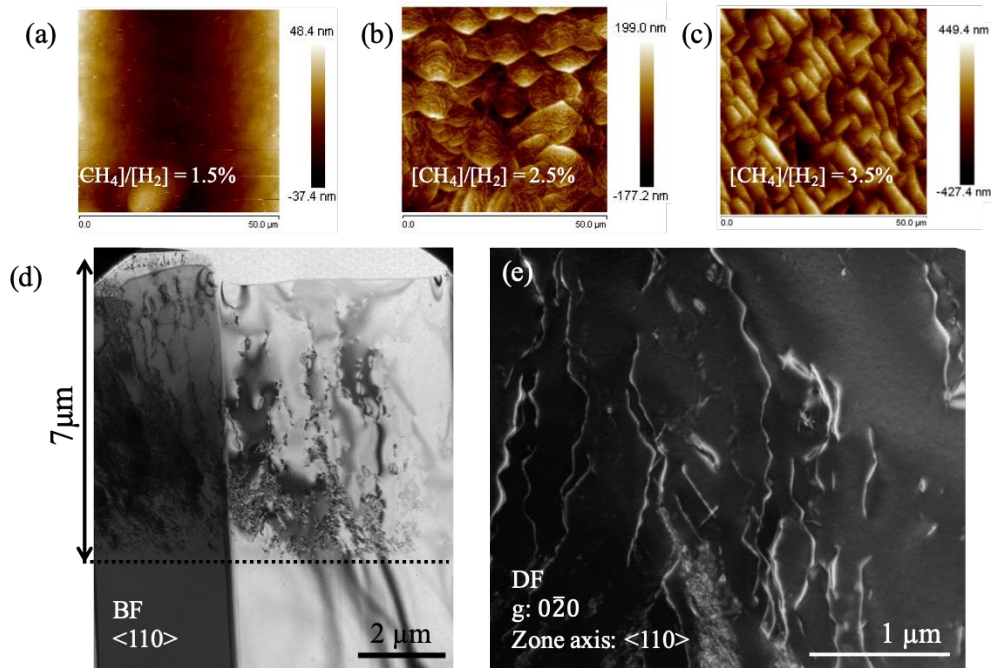


Figure 6: (a-c) AFM images of (100)-oriented P-doped diamond films grown at different methane concentrations. (d) BF micrograph of the *n*-type layer grown on a (100)-oriented *p*⁺/*p*⁻ stack layer, recorded on the <110> pole. The interface of the *n*-type layer is marked by a dashed line. (e) DF captured along the reflection $0\bar{2}0$, focusing on an area containing dislocations. Reproduced with permission from ref 52. Copyright 2023 Elsevier.

2.2.1.3 (110) orientation

Other orientations such as (110) were reported to exhibit elevated phosphorus concentrations, while they are much less stable growth fronts, so the layer grown on these orientations will likely result in a high defect density. The initial findings on the growth of (110)-oriented P-doped single crystal diamond layers revealed a significant increase in the root mean square roughness (R_{rms}) of the films when higher phosphine concentrations were introduced into the CVD plasma (Fig. 7). Therefore, it is plausible that the phosphine concentration may have an impact on the growth mechanism and potentially affect the deposition rate.

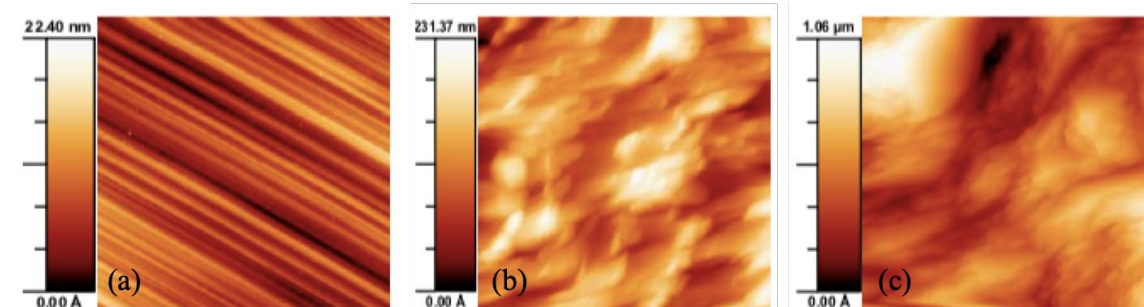


Figure 7: AFM images of (110)-oriented single crystal (a) diamond substrate with $R_{\text{rms}} \approx 3$ nm, P-doped diamond layer grown at (b) 500 ppm [P]/[C] ratio with $R_{\text{rms}} \approx 36$ nm, and (c) 1000 ppm [P]/[C] ratio with $R_{\text{rms}} \approx 0.18$ μm . The AFM images cover a scan area of 5×5 μm^2 . Reproduced with permission from ref 53. Copyright 2009 Ileana Andrada Lazea.

In 2016, we conducted a study on the CVD growth of a 66 μm thick homoepitaxial P-doped diamond on a (110)-oriented diamond substrate for the first time⁵⁴. Surprisingly, a very high deposition rate of 33 $\mu\text{m}/\text{h}$ was demonstrated, using a 1% methane concentration, surpassing the deposition rates recorded on P-doped (111)- and (100)-oriented crystals. We attributed this observation to the off-angle value (5° from (110) orientation), which was also found to significantly influence phosphorus incorporation. Furthermore, TEM showed a very low defect density, indicating the high crystalline quality of the grown CVD layer (Fig. 8(a)). Hall effect measurements were also performed. As depicted in Figure 8(b), a hopping mechanism was observed at temperatures below 450 K. The reported parameters include an activation energy of 0.56 eV, a donor concentration of $1.34 \times 10^{17} \text{ cm}^{-3}$, and a compensation ratio of 0.956. However, there is a discrepancy between the values of phosphorus content estimated by CL ($2.9 \times 10^{16} \text{ cm}^{-3}$) and SIMS ($4.8 \times 10^{16} \text{ cm}^{-3}$), and the donor concentration. We believe that this disparity could be related to (i) the CL and SIMS data only pertain to the topmost 800 nm and 4 μm from the surface, respectively, and (ii) potential inaccuracies in fitting as well as idiosyncrasies in the neutrality equation of the Hall effect.

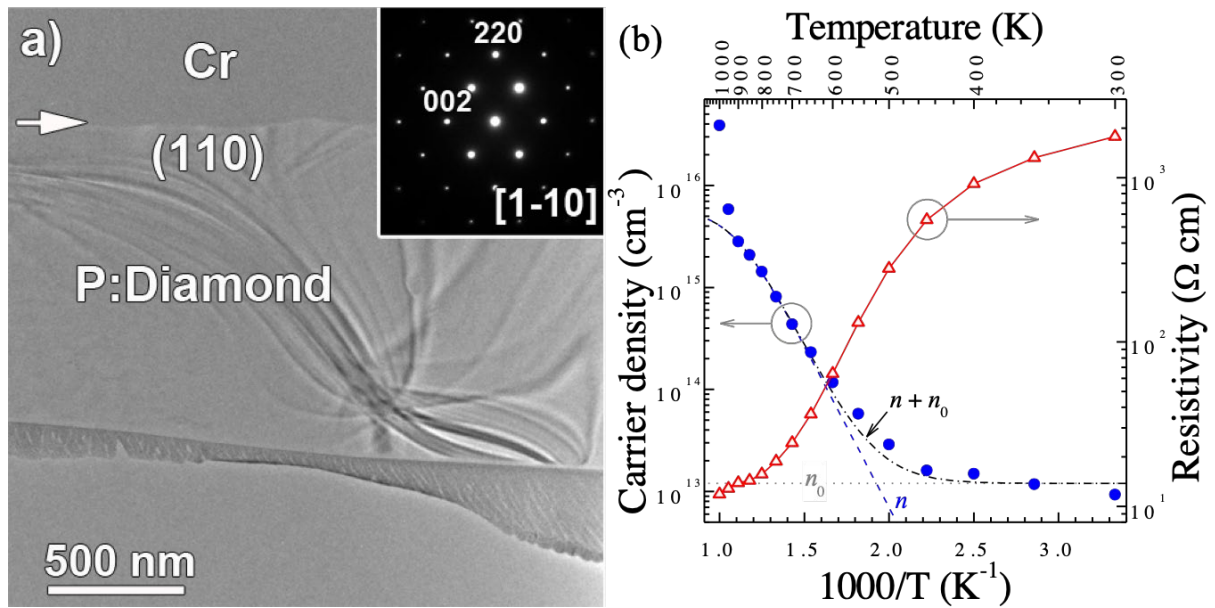


Figure 8: (a) BF TEM image and electron diffraction pattern (inset) with the absence of evidence of defects in the (110)-oriented P-doped diamond film. (b) Charge carrier density and resistivity as a function of temperature of the same sample. The dashed line shows the carrier density (n), the dotted line is the background carrier density due to hopping conduction (n_0), and the dashed-dotted line exhibits (n_0+n) . Reproduced with permission from ref 54. Copyright 2016 American Institute of Physics.

This work has been further explored to investigate the influence of the HPHT substrate's off-angle on both the phosphorus concentration and crystalline quality of (110)-oriented P-doped diamond films. As observed in the CL spectra of the samples measured at 5 K (Fig. 9), the full width at half maximum (FWHM) of the free-exciton assisted by a transverse optical (FE^{TO}) phonon increases from 0.022 eV to 0.037 eV as the substrate's off-angle is raised from 2.7° to 7.1° . As previously reported, the FWHM value of FE^{TO} peak is inherently linked to the crystalline quality of the film⁵⁵. A lower dislocation density corresponds to a narrower FWHM of the FE^{TO} peak. The phosphorus concentrations in the films were estimated to be approximately $1 \times 10^{17} \text{ cm}^{-3}$ by CL spectroscopy, nearly one order of magnitude higher than previous results. This concentration remained consistent for all three samples, regardless of the substrate's off-angle.

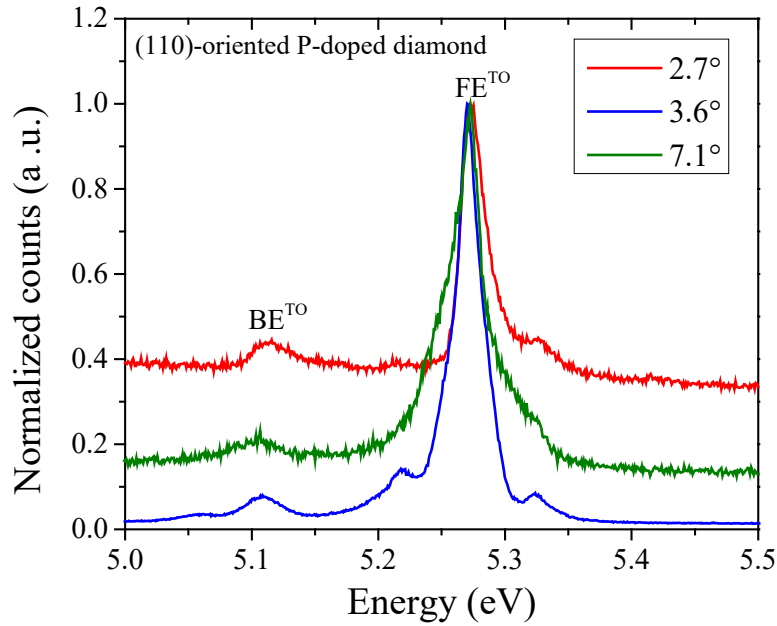


Figure 9: CL spectra of (110)-oriented P-doped single crystal diamond films deposited on HPHT substrates with off-angles of 2.7°, 3.6°, and 7.1°. The samples were grown at 0.15% [CH₄]/[H₂], 1000 ppm [P]/[C] ratio, and temperature of 1140°C for 4 hours. BE^{TO} is the neutral boron bound exciton assisted by a TO phonon.

3. Conclusions and outlook

In conclusion, our research endeavours have shed light on the remarkable potential of *n*-type CVD diamond, offering fresh perspectives in the world of semiconductor technology. Through our investigations, we have made significant strides in the development of high-quality *n*-type diamond films. By introducing nitrogen into the CVD plasma, we found a nuanced relationship between nitrogen concentration and film microstructure, leading to the formation of ultra-nanocrystalline diamond with profound implications for material properties. The exploration of methane concentration's role in the growth of N-incorporated NCD films revealed the potential for tailoring the crystalline quality and properties of these materials, including the realization of low-resistivity nanoneedles. For the P-doped polycrystalline diamond films, we achieved well-defined grain structures, although morphological imperfections and twin boundaries persist. The approximate phosphorus incorporation of 10¹⁹ cm⁻³ opens new dimensions for optimizing these films and their applications. Our foray into co-doping NCD films with nitrogen and phosphorus demonstrated a transition from microcrystalline diamond grains to nanocrystalline diamond structures, highlighting the versatility of *n*-type diamond and the intriguing properties of phosphorus as a donor dopant.

In (111)-oriented P-doped single crystal diamond films, the formation of crystal defects remains an area of concern. Achieving *n*-type conductivity in (100)-oriented diamond films presents an ongoing challenge, albeit one that we continued to address by exploring the influence of methane concentration on crystalline quality and phosphorus incorporation. Surprisingly, our findings in (110)-oriented P-doped single crystal diamond growth offer a promising avenue with notable deposition rates and low defect density.

Looking ahead, *n*-type CVD diamond growth advances, driving innovation in promising applications. However, key aspects need attention to reach its full potential:

- (1) **Enhancing *n*-type conductivity:** Despite recent advancements, attaining *n*-type conductivity remains a challenge, primarily due to compensation mechanisms. Understanding how compensation influences carrier concentration is crucial for optimizing diamond-based electronic devices. In this context, point defects in diamond such as hydrogen-passivated vacancies act as a strong donor compensation centre; therefore, remarkably reduce electron conductivity of diamond-based devices. This necessitates a meticulous understanding of the CVD growth conditions. This dual approach holds promise for advancing the performance of *n*-type diamond films in various applications.
- (2) **Grain boundary effects:** Grain boundaries can hinder charge carriers, causing non-uniform electronic behaviour, affecting semiconductor performance. The challenge is to understand and mitigate these effects, optimizing growth conditions for larger, uniform grains and minimizing grain boundary formation. Post-growth treatments and defect engineering enhance polycrystalline diamond's electrical properties, making it more accessible for innovative technologies.
- (3) **Scalability:** For upscaling diamond-based devices, especially in power electronics, heteroepitaxy is a compelling approach. However, the formidable challenge of dislocation density, needs attention. Investigating *n*-type diamond layers grown on freestanding heteroepitaxial diamond is essential to overcome this limitation.

Biographies

Rozita Rouzbahani earned her Ph.D. degree in 2021 from Hasselt University. She currently serves as a postdoctoral researcher, specializing in the CVD growth of doped single crystal diamond films, with a primary focus on the fabrication and characterization of diamond-based high-power electronics.

Kamatchi Jothiramalingam Sankaran is a Senior Scientist at CSIR-Institute of Minerals and Materials Technology, India, where he obtained his PhD degree in Materials Science and Engineering in 2013. He worked for five years as a postdoctoral researcher at Hasselt University. His research interests focus on the development, characterization and applications of electrically conducting diamond materials.

Paulius Pobedinskas is a Senior Researcher within the Wide Band Gap Material research group at Hasselt University, where he obtained his PhD degree in Physics in 2012. His background is in CVD diamond and III-V nitrides, synthesis and processing, structural and mechanical analysis of thin films, nanoscale physics, and numerical modelling.

Ken Haenen is a Full Professor of Experimental Physics at Hasselt University, Belgium, and guest professor at IMEC, Belgium. He has been working on *n*-type diamond since 1997, when he started his PhD, and currently leads the Wide Band Gap Materials research group at the Institute for Materials Research (IMO-IMOMECE). His research interests focus on CVD diamond, including deposition, opto-electronic characterisation, surface functionalisation, and diamond-based devices as part of a broader scope examining carbon materials for power generation and conversion.

Acknowledgments

The authors would like to thank all the current and former members of the Wide Band Gap Material group for their valuable contribution to these remarkable findings on the CVD growth of *n*-type diamond. The authors acknowledge Prof. Dr. David Eon at Université Grenoble-Alps, CNRS, Institut Néel, Grenoble, France for his contribution to the cathodoluminescence spectroscopy measurements. Financial support provided by the Research Foundation Flanders (FWO) in the form of project G0D4920N, the Special Research Fund (BOF) via the Methusalem NANO network are gratefully acknowledged.

References

- (1) Umezawa, H. Recent Advances in Diamond Power Semiconductor Devices. *Mater. Sci. Semicond. Process.* **2018**, *78*, 147–156. <https://doi.org/10.1016/j.mssp.2018.01.007>.
- (2) Schirhagl, R.; Chang, K.; Loretz, M.; Degen, C. L. Nitrogen-Vacancy Centers in Diamond: Nanoscale Sensors for Physics and Biology. *Annu. Rev. Phys. Chem.* **2014**, *65* (1), 83–105. <https://doi.org/10.1146/annurev-physchem-040513-103659>.
- (3) Childress, L.; Hanson, R. Diamond NV Centers for Quantum Computing and Quantum Networks. *MRS Bull.* **2013**, *38* (2), 134–138. <https://doi.org/10.1557/mrs.2013.20>.

- (4) Donato, N.; Rouger, N.; Pernot, J.; Longobardi, G.; Udrea, F. Diamond Power Devices: State of the Art, Modelling, Figures of Merit and Future Perspective. *J. Phys. D. Appl. Phys.* **2020**, *53* (9), 093001. <https://doi.org/10.1088/1361-6463/ab4eab>.
- (5) Berdermann, E.; Afanaciev, K.; Ciobanu, M.; Fischer, M.; Gsell, S.; Kiš, M.; Lagomarsino, S.; Lohmann, W.; Mayr, M.; Pomorski, M.; Rahman, M. S.; Schmidt, C. J.; Sciortino, S.; Schreck, M.; Stehl, C.; Träger, M. Progress in Detector Properties of Heteroepitaxial Diamond Grown by Chemical Vapor Deposition on Ir/YSZ/Si(001) Wafers. *Diam. Relat. Mater.* **2019**, *97*, 107420. <https://doi.org/10.1016/j.diamond.2019.05.006>.
- (6) Truscott, B. S.; Kelly, M. W.; Potter, K. J.; Ashfold, M. N. R.; Mankelevich, Y. A. Microwave Plasma-Activated Chemical Vapor Deposition of Nitrogen-Doped Diamond. II: CH₄/N₂/H₂ Plasmas. *J. Phys. Chem. A* **2016**, *120* (43), 8537–8549. <https://doi.org/10.1021/acs.jpca.6b09009>.
- (7) Ščajev, P.; Jurkevičius, J.; Mickevičius, J.; Jarašiūnas, K.; Kato, H. Features of Free Carrier and Exciton Recombination, Diffusion, and Photoluminescence in Undoped and Phosphorus-Doped Diamond Layers. *Diam. Relat. Mater.* **2015**, *57*, 9–16. <https://doi.org/10.1016/j.diamond.2015.02.003>.
- (8) Yang, L.; Fan, R.; Hu, A.; Ma, J.; Liu, Y.; Lu, Y. Tuning Donor Level of Nitrogen-Doped Diamond by Deep Strain Engineering—An Ab Initio Study. *Appl. Phys. Lett.* **2023**, *123* (6), 062105. <https://doi.org/10.1063/5.0159829>.
- (9) Pinault-Thaury, M.-A.; Stenger, I.; Gillet, R.; Temgoua, S.; Chikoidze, E.; Dumont, Y.; Jomard, F.; Kociniewski, T.; Barjon, J. Attractive Electron Mobility in (113) n-Type Phosphorus-Doped Homoepitaxial Diamond. *Carbon N. Y.* **2021**, *175*, 254–258. <https://doi.org/10.1016/j.carbon.2021.01.011>.
- (10) Haenen, K.; Meykens, K.; Nesládek, M.; Knuyt, G.; Quaeys, C.; Stals, L. M.; Koizumi, S.; Gheeraert, E. Low Temperature Photoconductivity Detection of Phosphorus in Diamond. *Phys. Status Solidi Appl. Res.* **1999**, *174* (1), 53–58. [https://doi.org/10.1002/\(SICI\)1521-396X\(199907\)174:1<53::AID-PSSA53>3.0.CO;2-9](https://doi.org/10.1002/(SICI)1521-396X(199907)174:1<53::AID-PSSA53>3.0.CO;2-9).
- (11) Miyazaki, T.; Okushi, H.; Uda, T. Shallow Donor State Due to Nitrogen-Hydrogen Complex in Diamond. *Phys. Rev. Lett.* **2002**, *88* (6), 066402. <https://doi.org/10.1103/PhysRevLett.88.066402>.
- (12) Lombardi, E. B.; Mainwood, A.; Osuch, K. Interaction of Hydrogen with Boron, Phosphorus, and Sulfur in Diamond. *Phys. Rev. B* **2004**, *70* (20), 205201.

<https://doi.org/10.1103/PhysRevB.70.205201>.

- (13) Araujo, D.; Suzuki, M.; Lloret, F.; Alba, G.; Villar, P. Diamond for Electronics: Materials, Processing and Devices. *Materials (Basel)*. **2021**, *14* (22), 7081. <https://doi.org/10.3390/ma14227081>.
- (14) Nebel, C.; Aharonovich, I.; Mizuochi, N.; Hatano, M. *Diamond for Quantum Applications Part I, Volume 103*, 1st ed.; Nebel, C. E., Aharonovich, I., Mizuochi, N., Hatano, M., Eds.; Elsevier: London, **2020**.
- (15) Sankaran, K. J.; Tai, N. H.; Lin, I. N. Microstructural Evolution of Diamond Films from CH₄/H₂/N₂ Plasma and Their Enhanced Electrical Properties. *J. Appl. Phys.* **2015**, *117* (7), 075303. <https://doi.org/10.1063/1.4913258>.
- (16) Afzal, A.; Rego, C. A.; Ahmed, W.; Cherry, R. I. HFCVD Diamond Grown with Added Nitrogen: Film Characterization and Gas-Phase Composition Studies. *Diam. Relat. Mater.* **1998**, *7* (7), 1033–1038. [https://doi.org/10.1016/S0925-9635\(98\)00148-4](https://doi.org/10.1016/S0925-9635(98)00148-4).
- (17) Chowdhury, S.; Borham, J.; Catledge, S. A.; Eberhardt, A. W.; Johnson, P. S.; Vohra, Y. K. Synthesis and Mechanical Wear Studies of Ultra Smooth Nanostructured Diamond (USND) Coatings Deposited by Microwave Plasma Chemical Vapor Deposition with He/H₂/CH₄/N₂ Mixtures. *Diam. Relat. Mater.* **2008**, *17* (4–5), 419–427. <https://doi.org/10.1016/j.diamond.2007.08.041>.
- (18) Hirai, H.; Kondo, K. I. Modified Phases of Diamond Formed under Shock Compression and Rapid Quenching. *Science*. **1991**, *253* (5021), 772–774. <https://doi.org/10.1126/science.253.5021.772>.
- (19) Kovarik, P.; Bourdon, E. B. D.; Prince, R. H. Electron-Energy-Loss Characterization of Laser-Deposited a -C, a -C:H, and Diamond Films. *Phys. Rev. B* **1993**, *48* (16), 12123–12129. <https://doi.org/10.1103/PhysRevB.48.12123>.
- (20) Praver, S.; Nugent, K. .; Jamieson, D. .; Orwa, J. .; Bursill, L. .; Peng, J. . The Raman Spectrum of Nanocrystalline Diamond. *Chem. Phys. Lett.* **2000**, *332* (1–2), 93–97. [https://doi.org/10.1016/S0009-2614\(00\)01236-7](https://doi.org/10.1016/S0009-2614(00)01236-7).
- (21) Arenal, R.; Bruno, P.; Miller, D. J.; Bleuel, M.; Lal, J.; Gruen, D. M. Diamond Nanowires and the Insulator-Metal Transition in Ultrananocrystalline Diamond Films. *Phys. Rev. B* **2007**, *75* (19), 195431. <https://doi.org/10.1103/PhysRevB.75.195431>.
- (22) Li, X.; Perkins, J.; Collazo, R.; Nemanich, R. J.; Sitar, Z. Investigation of the Effect of the Total Pressure and Methane Concentration on the Growth Rate and Quality of Diamond Thin Films Grown by MPCVD. *Diam. Relat. Mater.* **2006**, *15* (11-12 SPEC. ISS.), 1784–1788. <https://doi.org/10.1016/j.diamond.2006.09.008>.

- (23) Rakha, S. A.; Yu, G.; Cao, J.; He, S.; Zhou, X. Influence of CH₄ on the Morphology of Nanocrystalline Diamond Films Deposited by Ar Rich Microwave Plasma. *J. Appl. Phys.* **2010**, *107* (11), 114324. <https://doi.org/10.1063/1.3410804>.
- (24) Locher, R.; Wild, C.; Herres, N.; Behr, D.; Koidl, P. Nitrogen Stabilized $\langle 100 \rangle$ Texture in Chemical Vapor Deposited Diamond Films. *Appl. Phys. Lett.* **1994**, *65* (1), 34–36. <https://doi.org/10.1063/1.113064>.
- (25) Ashfold, M. N. R.; Mahoney, E. J. D.; Mushtaq, S.; Truscott, B. S.; Mankelevich, Y. A. What [Plasma Used for Growing] Diamond Can Shine like Flame? *Chem. Commun.* **2017**, *53* (76), 10482–10495. <https://doi.org/10.1039/C7CC05568D>.
- (26) Badzian, A.; Badzian, T.; Lee, S.-T. Synthesis of Diamond from Methane and Nitrogen Mixture. *Appl. Phys. Lett.* **1993**, *62* (26), 3432–3434. <https://doi.org/10.1063/1.109039>.
- (27) Sankaran, K. J.; Yeh, C.-J.; Hsieh, P.-Y.; Pobedinskas, P.; Kunuku, S.; Leou, K.-C.; Tai, N.-H.; Lin, I.-N.; Haenen, K. Origin of Conductive Nanocrystalline Diamond Nanoneedles for Optoelectronic Applications. *ACS Appl. Mater. Interfaces* **2019**, *11* (28), 25388–25398. <https://doi.org/10.1021/acsami.9b05469>.
- (28) Sankaran, K. J.; Huang, B.; Saravanan, A.; Manoharan, D.; Tai, N.; Lin, I. -N. Nitrogen Incorporated Ultrananocrystalline Diamond Microstructures From Bias-Enhanced Microwave N₂/CH₄-Plasma Chemical Vapor Deposition. *Plasma Process. Polym.* **2016**, *13* (4), 419–428. <https://doi.org/10.1002/ppap.201500079>.
- (29) Lazea, A.; Mortet, V.; D’Haen, J.; Geithner, P.; Ristein, J.; D’Olieslaeger, M.; Haenen, K. Growth of Polycrystalline Phosphorous-Doped CVD Diamond Layers. *Chem. Phys. Lett.* **2008**, *454* (4–6), 310–313. <https://doi.org/10.1016/j.cplett.2008.02.030>.
- (30) Janssen, W.; Turner, S.; Sakr, G.; Jomard, F.; Barjon, J.; Degutis, G.; Lu, Y.-G.; D’Haen, J.; Hardy, A.; Bael, M. Van; Verbeeck, J.; Tendeloo, G. Van; Haenen, K. Substitutional Phosphorus Incorporation in Nanocrystalline CVD Diamond Thin Films. *Phys. status solidi - Rapid Res. Lett.* **2014**, *8* (8), 705–709. <https://doi.org/10.1002/pssr.201409235>.
- (31) Mary Joy, R.; Pobedinskas, P.; Baule, N.; Bai, S.; Jannis, D.; Gauquelin, N.; Pinault-Thaury, M.-A.; Jomard, F.; Sankaran, K. J.; Rouzbahani, R.; Lloret, F.; Desta, D.; D’Haen, J.; Verbeeck, J.; Becker, M. F.; Haenen, K. The Effect of Microstructure and Film Composition on the Mechanical Properties of Linear Antenna CVD Diamond Thin Films. *Acta Mater.* **2024**, *264*, 119548. <https://doi.org/10.1016/j.actamat.2023.119548>.
- (32) Haenen, K.; Lazea, A.; Barjon, J.; D’Haen, J.; Habka, N.; Teraji, T.; Koizumi, S.; Mortet, V. P-Doped Diamond Grown on (110)-Textured Microcrystalline Diamond:

- Growth, Characterization and Devices. *J. Phys. Condens. Matter* **2009**, *21* (36), 364204. <https://doi.org/10.1088/0953-8984/21/36/364204>.
- (33) Habka, N.; Barjon, J.; Lazea, A.; Haenen, K. Stress in (110)-Textured Phosphorus-Doped Polycrystalline Diamond Studied by Raman and Cathodoluminescence Spectroscopies. *J. Appl. Phys.* **2010**, *107* (10), 103531. <https://doi.org/10.1063/1.3428452>.
- (34) Drijkoningen, S.; Pobedinskas, P.; Korneychuk, S.; Momot, A.; Balasubramaniam, Y.; Van Bael, M. K.; Turner, S.; Verbeeck, J.; Nesládek, M.; Haenen, K. On the Origin of Diamond Plates Deposited at Low Temperature. *Cryst. Growth Des.* **2017**, *17* (8), 4306–4314. <https://doi.org/10.1021/acs.cgd.7b00623>.
- (35) Lloret, F.; Sankaran, K. J.; Millan-barba, J.; Desta, D. Improved Field Electron Emission Properties of Phosphorus and Nitrogen Co-Doped Nanocrystalline Diamond Films. **2020**, *10* (6), 1024. <https://doi.org/10.3390/nano10061024>.
- (36) Koizumi, S.; Kamo, M.; Sato, Y.; Ozaki, H.; Inuzuka, T. Growth and Characterization of Phosphorous Doped {111} Homoepitaxial Diamond Thin Films. *Appl. Phys. Lett.* **1997**, *71* (8), 1065–1067. <https://doi.org/10.1063/1.119729>.
- (37) Koizumi, S.; Teraji, T.; Kanda, H. Phosphorus-Doped Chemical Vapor Deposition of Diamond. *Diam. Relat. Mater.* **2000**, *9* (3–6), 935–940. [https://doi.org/10.1016/S0925-9635\(00\)00217-X](https://doi.org/10.1016/S0925-9635(00)00217-X).
- (38) Katagiri, M.; Isoya, J.; Koizumi, S.; Kanda, H. Lightly Phosphorus-Doped Homoepitaxial Diamond Films Grown by Chemical Vapor Deposition. *Appl. Phys. Lett.* **2004**, *85* (26), 6365–6367. <https://doi.org/10.1063/1.1840119>.
- (39) Kato, H.; Futako, W.; Yamasaki, S.; Okushi, H. Homoepitaxial Growth and Characterization of Phosphorus-Doped Diamond Using Tertiarybutylphosphine as a Doping Source. *Diam. Relat. Mater.* **2004**, *13* (11–12), 2117–2120. <https://doi.org/10.1016/j.diamond.2004.07.010>.
- (40) Koizumi, S. Growth and Characterization of Phosphorus Doped N-Type Diamond Thin Films. *Phys. status solidi* **1999**, *172* (1), 71–78. [https://doi.org/10.1002/\(SICI\)1521-396X\(199903\)172:1<71::AID-PSSA71>3.0.CO;2-N](https://doi.org/10.1002/(SICI)1521-396X(199903)172:1<71::AID-PSSA71>3.0.CO;2-N).
- (41) Nesládek, M.; Meykens, K.; Haenen, K.; Stals, L. M.; Teraji, T.; Koizumi, S. Low-Temperature Spectroscopic Study of n-Type Diamond. *Phys. Rev. B* **1999**, *59* (23), 14852–14855. <https://doi.org/10.1103/PhysRevB.59.14852>.
- (42) Haenen, K.; Meykens, K.; Nesládek, M.; Knuyt, G.; Stals, L. M.; Teraji, T.; Koizumi, S. Electronic Structure of Phosphorus in N-Type CVD Diamond Films: Revised. *Phys.*

- Status Solidi Appl. Res.* **2000**, *181* (1), 11–16. [https://doi.org/10.1002/1521-396X\(200009\)181:1<11::AID-PSSA11>3.0.CO;2-W](https://doi.org/10.1002/1521-396X(200009)181:1<11::AID-PSSA11>3.0.CO;2-W).
- (43) Gheeraert, E.; Koizumi, S.; Teraji, T.; Kanda, H.; Nesladek, M. Electronic States of Phosphorus in Diamond. *Diam. Relat. Mater.* **2000**, *9* (3–6), 948–951. [https://doi.org/10.1016/S0925-9635\(99\)00225-3](https://doi.org/10.1016/S0925-9635(99)00225-3).
- (44) Haenen, K.; Nesládek, M.; De Schepper, L.; Kravets, R.; Vaněček, M.; Koizumi, S. The Phosphorous Level Fine Structure in Homoepitaxial and Polycrystalline N-Type CVD Diamond. *Diam. Relat. Mater.* **2004**, *13* (11–12), 2041–2045. <https://doi.org/10.1016/j.diamond.2004.06.016>.
- (45) Grotjohn, T. A.; Tran, D. T.; Yaran, M. K.; Demlow, S. N.; Schuelke, T. Heavy Phosphorus Doping by Epitaxial Growth on the (111) Diamond Surface. *Diam. Relat. Mater.* **2014**, *44*, 129–133. <https://doi.org/10.1016/j.diamond.2014.02.009>.
- (46) Fedyanin, D. Y.; Agio, M. Ultrabright Single-Photon Source on Diamond with Electrical Pumping at Room and High Temperatures. *New J. Phys.* **2016**, *18* (7), 073012. <https://doi.org/10.1088/1367-2630/18/7/073012>.
- (47) Flatae, A. M.; Lagomarsino, S.; Sledz, F.; Soltani, N.; Nicley, S. S.; Haenen, K.; Rechenberg, R.; Becker, M. F.; Sciortino, S.; Gelli, N.; Giuntini, L.; Taccetti, F.; Agio, M. Silicon-Vacancy Color Centers in Phosphorus-Doped Diamond. *Diam. Relat. Mater.* **2020**, *105*, 107797. <https://doi.org/10.1016/j.diamond.2020.107797>.
- (48) Kato, H.; Yamasaki, S.; Okushi, H. N -Type Doping of (001)-Oriented Single-Crystalline Diamond by Phosphorus. *Appl. Phys. Lett.* **2005**, *86* (22) , 222111. <https://doi.org/10.1063/1.1944228>.
- (49) Haenen, K.; Meykens, K.; Nesládek, M.; Knuyt, G.; Stals, L. M.; Teraji, T.; Koizumi, S.; Gheeraert, E. Phonon-Assisted Electronic Transitions in Phosphorus-Doped n-Type Chemical Vapor Deposition Diamond Films. *Diam. Relat. Mater.* **2001**, *10* (3–7), 439–443. [https://doi.org/10.1016/S0925-9635\(00\)00511-2](https://doi.org/10.1016/S0925-9635(00)00511-2).
- (50) Haenen, K.; Meykens, K.; Nesládek, M.; Knuyt, G.; Stals, L. M.; Teraji, T.; Koizumi, S.; Gheeraert, E. Temperature Dependent Spectroscopic Study of the Electronic Structure of Phosphorus in N-Type CVD Diamond Films. *Diam. Relat. Mater.* **2000**, *9* (3–6), 952–955. [https://doi.org/10.1016/S0925-9635\(99\)00202-2](https://doi.org/10.1016/S0925-9635(99)00202-2).
- (51) Rouzbahani, R.; Nicley, S. S.; Vanpoucke, D. E. P.; Lloret, F.; Pobedinskas, P.; Araujo, D.; Haenen, K. Impact of Methane Concentration on Surface Morphology and Boron Incorporation of Heavily Boron-Doped Single Crystal Diamond Layers. *Carbon N. Y.* **2021**, *172*, 463–473. <https://doi.org/10.1016/j.carbon.2020.10.061>.

- (52) Lloret, F.; Soto, B.; Rouzbahani, R.; Gutiérrez, M.; Haenen, K.; Araujo, D. High Phosphorous Incorporation in (100)-Oriented MP CVD Diamond Growth. *Diam. Relat. Mater.* **2023**, *133*, 109746. <https://doi.org/10.1016/j.diamond.2023.109746>.
- (53) Lazea, A. Growth and Characterization of Phosphorus Doped N-Type CVD Diamond Films of Various Orientations and Devices/Applications Based on These, Hasselt University, **2009**. <http://hdl.handle.net/1942/21062>.
- (54) Balasubramaniam, Y.; Pobedinskas, P.; Janssens, S. D.; Sakr, G.; Jomard, F.; Turner, S.; Lu, Y.-G.; Dexters, W.; Soltani, A.; Verbeeck, J.; Barjon, J.; Nesládek, M.; Haenen, K. Thick Homoepitaxial (110)-Oriented Phosphorus-Doped n -Type Diamond. *Appl. Phys. Lett.* **2016**, *109* (6), 062105. <https://doi.org/10.1063/1.4960970>.
- (55) Ghodbane, S.; Omnès, F.; Agnès, C. A Cathodoluminescence Study of Boron Doped {111}-Homoepitaxial Diamond Films. *Diam. Relat. Mater.* **2010**, *19* (4), 273–278. <https://doi.org/10.1016/j.diamond.2009.11.003>.